PREPARATION OF COMPOSITE FILAMENTS AND 3D PRINTS BASED ON PLA MODIFIED WITH CARBON MATERIALS WITH THE POTENTIAL APPLICATIONS IN TISSUE ENGINEERING

Martyna Hunger[1], Wiktor Podgórny[2], Aneta Frączek-Szczypta[1]*

AGH University of Science and Technology,
Al. Mickiewicza 30, 30-059 Krakow, Poland
[1] Faculty of Materials Science and Ceramics,
Department of Biomaterials and Composites,
[2] Faculty of Electrical Engineering Automatics,
Computer Science and Biomedical Engineering,
*e-mail: afraczek@agh.edu.pl

Abstract

This paper discusses the possibilities of obtaining polylactide-based composites and nanocomposites modified with carbon materials using the extrusion method, as well as the potential of their application in 3D printing technology. The aim of this research is to determine the impact of the presence of carbon additives on the properties of composites: mechanical, thermal and chemical. For this purpose, several research techniques were used such as scanning electron microscopy (SEM), X-ray photoelectron spectroscopy (XPS), DSC/TG analysis, infrared Fourier-transform infrared spectroscopy (FTIR) and mechanical tests. It has been shown that it is possible to effectively produce composite materials based on PLA and carbon modifiers after optimization of the extrusion and printing process. Special attention should be paid to the quality of carbon phases homogenization in PLA matrix because the inappropriate dispersion may have a negative effect on the final properties of the composite, especially those modified with nanomaterials. Moreover, the reinforcing effect of carbon phases can be observed, and the quality of obtained filament with carbon fiber after recycling does not differ significantly from the quality of commercially available filaments. The obtained filament was successfully used to print three-dimensional scaffolds. Therefore, both the use of materials which are biodegradable and biocompatible with human tissue and the 3D printing method have the potential to be applied in tissue engineering.

Keywords: *3D printing, poly(lactic acid), carbon materials, scaffold, tissue engineering*

[Engineering of Biomaterials 147 (2018) 7-15]

Introduction

In recent years, composite and nanocomposite materials have been very common due to the unique properties and a very wide range of applications - from technology, industry [1] to medicine and tissue engineering [2-4]. In the latter, biodegradable polymers such as polylactide (PLA) [5-10] or polycaprolactone (PCL) [11-15] deserve special attention. PLA is a thermoplastic polymer that can be obtained from renewable sources [16]. It is popular in biomedical applications due to its relatively good mechanical properties, biocompatibility and biodegradability, as well as simple processing and modification [17,18].

The disadvantage of polymers as biomaterials is frequently too rapid degradation in the physiological environment [19], insufficient mechanical strength and considerable deformability. However, the possibility of introducing modifications makes these materials predominant among the other typically used, e.g. metals [20]. Carbon materials like carbon fibers [21,22] and carbon nanomaterials, such as graphene [23], graphene oxide [12] or carbon nanotubes [24,25] are widely used as additives in polymer composites. Carbon materials are biocompatible with human tissues. They have antibacterial properties, high mechanical strength, and relatively low density. Those properties make the materials very beneficial modifying agents for tissue engineering [26].

There are many traditional methods of composite and nanocomposite biomaterials producing and molding [27]. However, the 3D printing technology, especially Fused Deposition Modeling (FDM) is relatively new and innovative [28]. It is a method of additive manufacturing, waste-free and rapid prototyping, which in general consists in applying subsequent layers of thermoplastic material to the substrate, based on the digital model. A filament with a certain diameter produced by extrusion is used as a semi-finished product. The advantage of additive production in comparison to the standard methods is controllable porosity, individualization of printed objects (patient-specific designs) and a favorable time-cost relation of manufacturing [29,30].

The aim of this research was to determine the effectiveness of extrusion in preparation of composite filaments and assessment of 3D printing (FDM) capabilities in manufacturing composite scaffolds based on carbon fibers and carbon nanomaterials for tissue engineering.

Materials and Methods

Materials

Poly(lactic acid) filament (Barrus Filaments, Holland, d = 1.75 ± 0.05 mm; PLA) was used in this study. The PLA properties are shown in TABLE 1. A commercial filament of poly(lactic acid) with short carbon fiber (Carbon Fiber PLA, Proto-Pasta, USA, 15% w/w SCF, d = 1.75 +/- 0.05 mm; PLA/SCF_C) was used as a reference material. To produce a composite filament, short carbon fibers (SCF_R) were used from the polyacrylonitrile precursor after thermal recycling (SGL Carbon Group, Poland, l = 6 and 12 mm), which were then milled and pressed (FIG. 1). In order to improve homogenization of the carbon fibers with polymer and obtain composite filaments, grinding and pressing of carbon fibers were performed in the PULVERISETTE 16 (Fritsch®) cross-beating mill and on a hand press at 20 MPa, respectively. Graphene oxide (GO) and multi-wall carbon nanotubes functionalized with hydroxyl groups (MWCNT-OH) were obtained from Nanostructured & Amorphous Materials, Inc. (USA). Selected data characterizing carbon nanomodifiers are presented in TABLES 2 and 3.

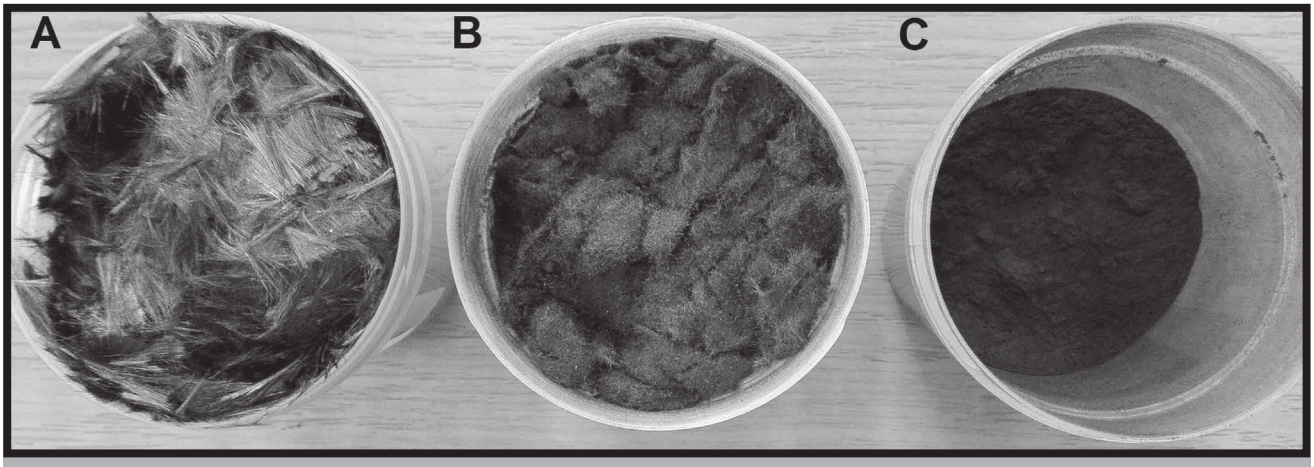

FIG. 1. Carbon fibers after recycling: A) before grinding, B) milled, C) pressed.

TABLE 1. PLA filament properties [31].

Dimensions	
Diameter	**Roundness**
1.75 ± 0.05 mm	≥ 95%
Physical properties	
Specific weight	1.24 g/cm^3
Thermal properties	
Printing temperature	180-210°C
Melting point	145-160°C
Vicat softening temperature	± 60°C

TABLE 2. GO characterization [32].

Purity	> 99 wt%
Diameter	0.5-3 µm
Thickness	0.55-1.2 nm
The number of layers	1-10
Density (at 20°C)	2.1 g/cm^3

TABLE 3. MWCNTs-OH characterization [32].

Purity	> 95 wt%	
Outer diameter	10-20 µm	
Inner diameter	5-10 nm	
Length	0.5-2 µm	
SSA	> 200 m^2/g	
Density (at 20°C)	2.1 g/cm^3	
Content of functional groups [%]	Multi-walled carbon nanotubes (without –OH)	> 95
	-OH	2.91-3.21

TABLE 4. Parameters of the extrusion process.

Nozzle	Custom in-line nozzle, tapering
Extrusion temperature	180°C
Extrusion speed	40 m/h
Diameter of the nozzle	1.75 mm

Methods

Extrusion – filament manufacturing

The extrusion process was carried out using a Filabot extruder (MakerBot®, USA). TABLE 4 presents the parameters of the extrusion process. The commercial PLA filament was cut into small pieces and 50 g of this polymer was introduced into 3 containers to obtain composite PLA filaments with the following additions: SCF_R (15% w/w of PLA; PLA/SCF_R), GO (1% w/w of PLA; PLA/GO) and MWCNT-OH (1% w/w of PLA; PLA/CNT). All the samples were mechanically mixed for 10 min. Each of the obtained mixtures was introduced into the extruder chamber, from where the material in the molten form was transported to the nozzle outlet, and then extruded as a bundle of the filament with a diameter of 1.75 mm. The material was formed in a gravitational manner (the beam freely dropped from a height of 40 cm to a flat surface, self-curling), while the formed material was air-cooled. In each case, the triple extrusion was performed (by re-cutting the obtained filament) to homogenize the materials more efficiently. In addition, pure PLA was also extruded in the same way in order to investigate the influence of extrusion process conditions on the structure and properties of the pure polymer.

3D printing

MakerBot Replicator 2X printer (MakerBot®, USA), based on FDM method was used to the 3D printing of scaffolds. The samples for testing were of a dog-bone shape (FIG. 2) with a 20% hexagonal filling. The purpose of creating such a shape of samples was to assess the possibilities of 3D printing of composite and nanocomposite filaments as well as to evaluate the mechanical properties of the obtained prints. Parameters of the printing process are shown in TABLE 5.

For the selected filaments, test prints of 3D scaffolds were also made. In order to create a correct scaffold model consistent with the assumptions, Autodesk Inventor® Professional 2017 was used. It is software with professional tools that enable 3D design of mechanical elements, their documentation and simulation of products. For the needs of the work, basic functions of the software were used, i.e. tools for parametric 3D design. Designs of the scaffolds serving as the basis for the prints are shown in FIG. 3.

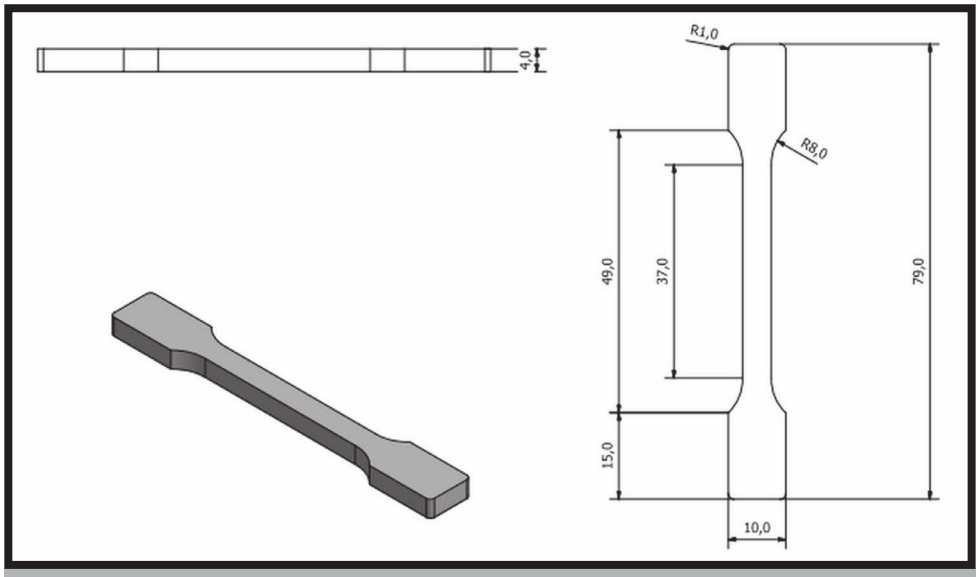

FIG. 2. Sample design (dog-bone) used for 3D printing.

TABLE 5. Parameters of 3D printing process.

Extruder temperature	200°C (PLA) 220°C (composites)
Platform temperature	30°C
Nozzle diameter	0.3 mm
Printing speed	50 mm/s (PLA) 35 mm/s (composites)
Layer height	0.2 mm
Number of shells	2
Thickness of external layers (top and bottom)	0.6 mm
Parameters of the sample (dogbone shape)	
Sample dimensions	79x10/5x4 mm
Infill	hexagonal
Infill density	20%

Characterization of carbon materials

The microstructure characterization of carbon additives was performed using SEM images (NOVA NanoSEM 200 (FEI™)) were made to measure fiber diameters and lengths after recycling and to compare them to commercial filament fibers, as well as to determine the fiber reinforcement effect. To check PLA matrix reinforcement effect, critical lengths of the fibers for both SCF_R and SCF_C were calculated. For this purpose, the formula 1 was used [49]:

$$l_{cr} = \frac{R_m d_m}{2\tau_o} \quad (1)$$

R_m – matrix strength [MPa]
(value given by the producer $R_m \approx 130$ MPa),
d_m – fiber diameter [μm],
τ_o – shear strength of the matrix (for PLA ~ 20 MPa)

Determination of the critical fiber length, above which the material strengthens, allowed determining which carbon fibers fulfil the criterion:

$$l_{cr} < l < 10\, l_{cr} \quad (2)$$

l_{cr} – critical fiber length, l – fiber length

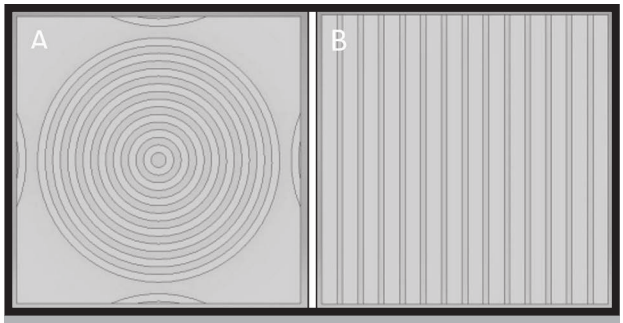

FIG. 3. Scaffolds designed in the Autodesk Inventor® Professional 2017 program: A) ring, B) linear.

XPS (Scanning XPS Microprobe PHI 5000 VersaProbell) was used to perform quantitative analysis of the chemical composition and to determine the types of chemical bonds occurring between elements on the surface of the tested carbon materials. The source of X-ray radiation was monochromatic Al Kα. The diameter of the beam was 100 μm, and the analysis surface φ 100 μm (25 W (4 mA, 15 kV)) at the charge neutralization Ar^+ -8 eV, e^- -1 eV. The analyzer resolution for the reference and detailed spectra was 117 eV and 46,95 eV, respectively.

Characterization of filaments

Having obtained the filaments, their diameters were measured and a macroscopic evaluation was made. Microscopic observations using SEM (NOVA NanoSEM 200 (FEI™)) were also performed to analyze the distribution of carbon phases in the polymer matrix.

Additionally, a static tensile test was carried out (Zwick 1435, Germany). Properties such as tensile strength, Young's modulus, relative strain and rupture work were evaluated. Parallel specimen length and the test speed were 40 mm and 50 mm/min, respectively. The Young's modulus determination was measured in the range of 30-50 N.

FTIR (Bruker Tensor 27 FTIR-ATR) was used to check and determine possible structural changes of the polymer as a result of several thermal treatments (thermal degradation) as well as changes caused by the presence of carbon additives (in particular nanomaterials). The wavelength range was between 4000 and 500 cm^{-1}, and the number of scans was 64. The test in the absorption mode was carried out using a diamond crystal, by Attenuated Total Reflectance (ATR).

DSC/TG measurements were made with the NETZSCH STA 449 F3 Jupiter®. The temperature of the test ranged from 40 to 600°C, while the heating rate was 10 K/min. In the DSC part graphs of the heat flow versus temperature were recorded, while in the TG part - the relation between the percentage loss of mass and temperature.

Characterization of the samples after printing

The printed samples shaped as dog-bones were evaluated macroscopically and compared in various aspects. To assess the practical obtaining possibilities of the samples, they were examined for mechanical properties. The static tensile test was performed in the same way as it was conducted on filaments (section 2.2.4).

Characterization of three-dimensional scaffolds

Measurements and macroscopic observations were also run on printed scaffolds. The comparative evaluation of the actual prints and the digital models was performed via microscopic observation and dimensional analysis (Keyence VHX-900F digital microscope). The tested parameter was the height of the scaffolds, measured on the basis of 3D images using tools that allow microscopic measurements attached as microscope software.

Results and Discussion

On the basis of SEM measurements (FIG. 4) it can be concluded that the manual pressing caused changes in the length of the fibers. On average, SCF_C lengths are almost twice as short as the SCF_R ones. In both cases, a significant length distribution is seen, although the SCF_R are more homogeneous. Determination of critical lengths based on the formula 1 led to the conclusion that carbon fibers obtained from both the commercial filament and the recycled filament meet the criterion (formula 2) providing the proper material reinforcement.

XPS measurement results (TABLE 6) determined the chemical composition on the surface of SCF_C, SCF_R, MWCNTs-OH and GO. Analysis of chemical states of C1s in carbon fibers showed their higher content in SCF_R. SCF_C were obtained for testing by dissolving the polymer matrix and could have a polymer on their surface.

TABLE 6. Atomic concentration of elements measured on the surface of the carbon materials.

Sample	C [%]	O [%]	N [%]
SCF_C	76.11	22.61	1.06
SCF_R	88.47	7.90	3.61
MWCNTs-OH	97.20	2.76	0.00
GO	66.83	31.26	1.30

Images of the obtained filaments are shown in FIG. 5. The similarity of PLA/SCF_R to PLA/SCF_C is noticeable. The average of the filament diameter value PLA/SCF_R was the closest to the diameter of the commercial filament (TABLE 7). Relatively low standard deviation shows a high homogeneity of the diameter along the entire length of the filament. The worst geometric parameters show PLA/GO. Its diameter had the lowest value, and the standard deviation was relatively high, which indicates a heterogeneity along the length of the filament. This is most likely due to the lack of sufficient homogenization of the GO in the sample. Graphene oxide tends to agglomeration and is less wetted by the polymer than other additives.

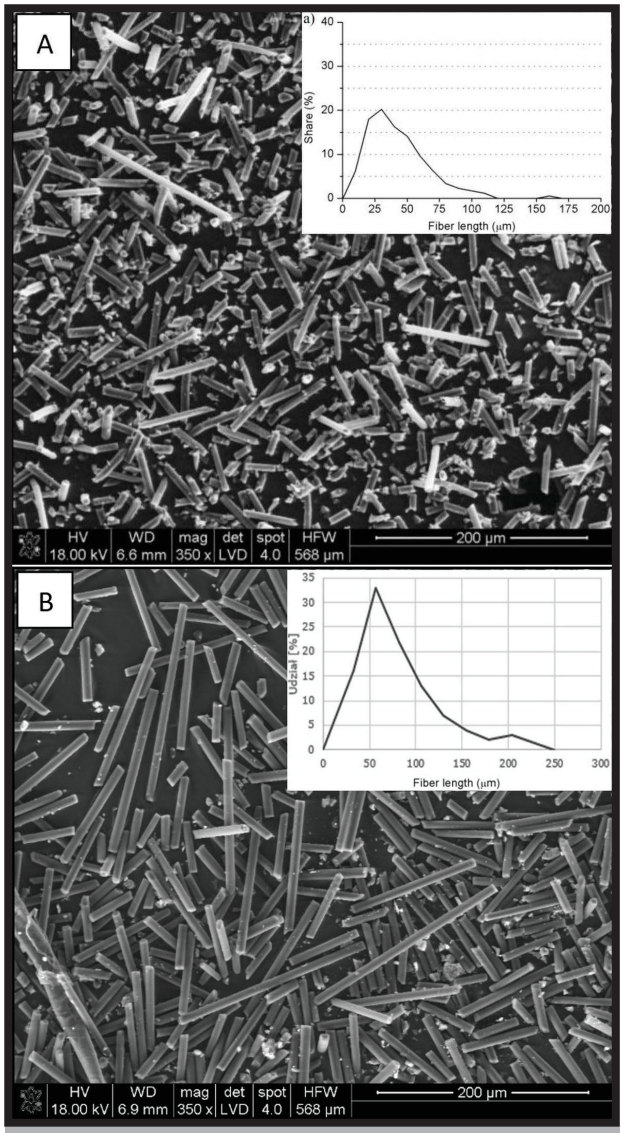

FIG. 4. SEM images (mag. 350x) and histograms: A) SCF_R, B) SCF_C.

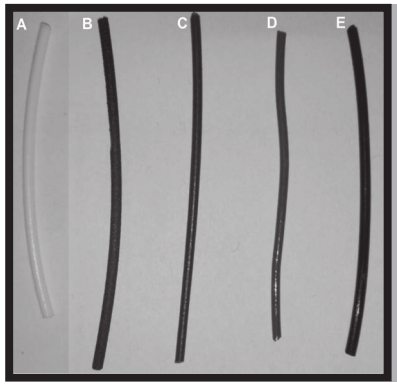

FIG. 5. Images of fragments of the obtained filaments: A) PLA, B) PLA/SCF_C, C) PLA/SCF_R, D) PLA/GO, E) PLA/CNT.

TABLE 7. Values of diameters of the obtained and the commercial filaments.

Filament	Diameter ± SD [mm]
PLA	1.75 ± 0.05
PLA/SCF_C	1.75 ± 0.05
PLA/SCF_R	1.57 ± 0.06
PLA/GO	1.41 ± 0.12
PLA/CNT	1.54 ± 0.09

SEM images of filaments cross-sections are shown in FIG 6. The images show that PLA/SCF_C has the best distribution of the reinforcing phase, and the homogenization of fibers for PLA/SCF_R is similar. Much worse distribution of the reinforcing phase is observed in the polymer nanocomposites. On the PLA/GO and PLA/CNT cross-sections (FIG. 6b and 6d), both the areas with larger agglomerates of the nanomaterial (black circles), as well as areas without modifying phase in form of agglomerates (white circles) are visible.

The results of mechanical tests are presented in TABLE 8. Among the obtained composites filaments, PLA/CNT has the highest tensile strength and this value is the same as for PLA/SCF_C. In turn, the nanotubes due to their characteristic structure transfer stresses better than graphene oxide. PLA/GO shows the lowest tensile strength and Young's modulus, which probably results from poor GO homogenization in the polymer matrix. On the basis of the obtained results, it can also be concluded that the production of filament PLA/SCF_R by extrusion is effective. Its tensile strength does not differ significantly from the commercial PLA/SCF_C filament. Only Young's modulus is about 30% lower in comparison with commercial filament (PLA/SCF_C). For this reason, a filament with recycled carbon fibers can be used to obtain materials that do not require the transfer of large forces. One such application can be scaffolds for tissue regeneration, taking into account the biocompatibility of carbon fibers.

TABLE 8. Results after tensile test of filaments.

	R_m ± SD [MPa]	Young's Modulus ±SD [GPa]	Strain ε ± SD [%]	Rupture work ± SD [N·mm]
PLA	59.88 ± 5.26	2.92 ± 0.17	2.80 ± 0.43	79.96 ± 20.16
PLA/SCF_C	62.63 ± 6.59	5.15 ± 0.64	1.71 ± 0.22	59.52 ± 13.61
PLA/SCF_R	60.30 ± 6.82	3.60 ± 0.81	2.58 ± 0.75	75.97 ± 29.25
PLA/GO	52.58 ± 5.98	2.04 ± 0.30	4.24 ± 0.92	90.01 ± 35.45
PLA/CNT	62.00 ± 4.65	2.68 ± 0.27	3.14 ± 0.11	77.12 ± 9.26

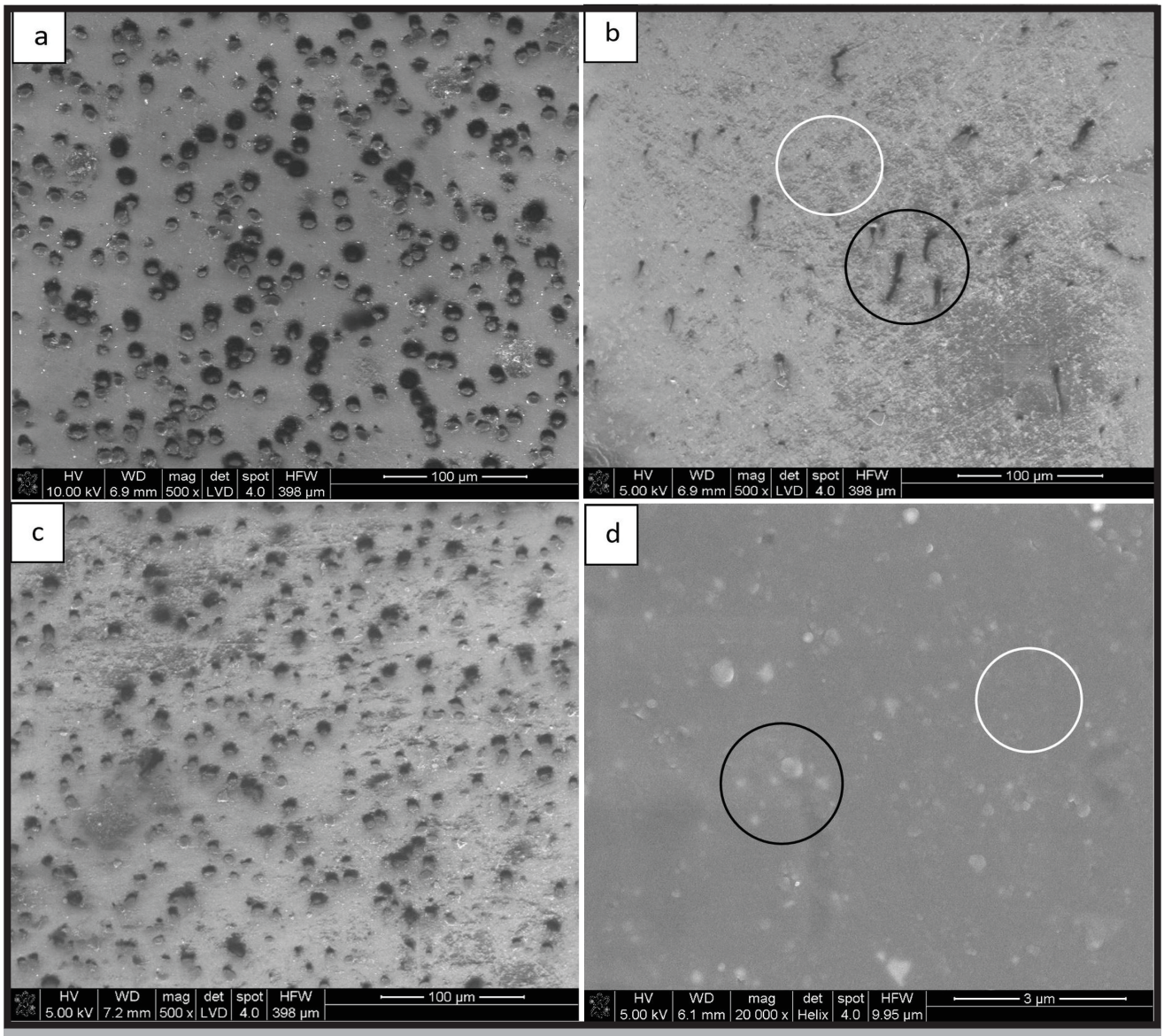

FIG. 6. SEM images of the filament cross-sections: a) PLA/SCF_C (mag. 500x), b) PLA/GO (mag. 500x), c) PLA/SCF_R (mag. 500x), d) PLA/CNT (mag. 20000x).

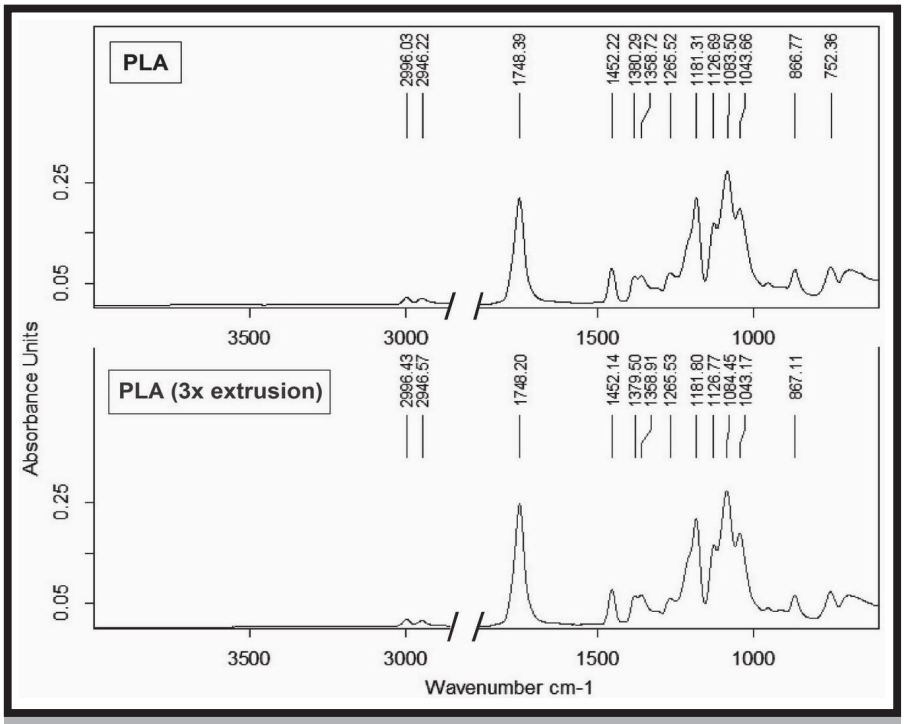

FIG. 7. FTIR spectrum for PLA and PLA after triple extrusion.

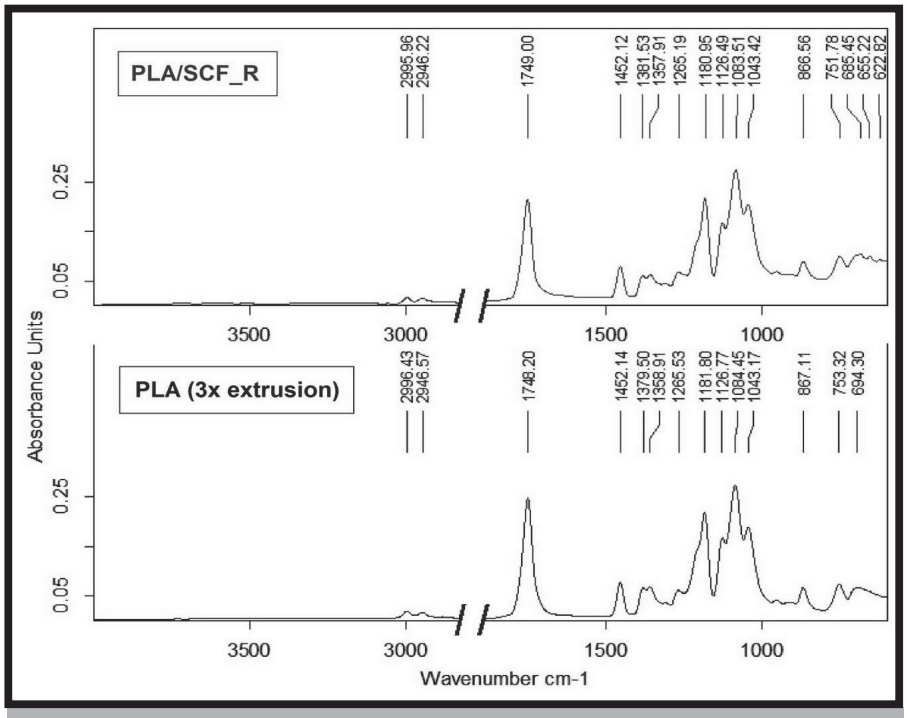

FIG. 8. FTIR spectrum for PLA/SCF_R and PLA after triple extrusion.

FTIR-ATR spectroscopic measurements did not show the effect of both the temperature during the triple extrusion and the presence of carbon additives on structural changes of PLA. Comparative spectra for PLA with PLA after triple extrusion and PLA after triple extrusion with PLA/SCF_R are shown in FIGs 7 and 8, respectively. They do not show significant changes in spectra - characteristic bands occur at the same wavelengths. The characteristic band at the 1748 cm^{-1} is derived from the stretching vibrations of C=O. In turn, the bands at the wavenumbers 1181 and 1083 cm^{-1} are the result of the stretching vibrations coming from the single C-O bond. The subtle bands at 1452 cm^{-1}, 1380 cm^{-1}, and 1358 cm^{-1} are derived from the bond of C-H.

DSC/TG tests showed an insignificant impact of the triple extrusion and the presence of carbon additives on the characteristic temperatures of PLA (FIG. 9 and 10). The DSC results for the PLA and PLA after triple extrusion show that the thermal processing of the polymer has an impact on reducing the degradation temperature about 20°C. From the TG plot for filaments with carbon fiber PLA/SCF_C and PLA/SCF_R, it appears that residues at 600°C were 15.20 and 13.14%, respectively (FIG. 11). Taking into account the assumed concentration of carbon phases (15% w/w), it can be concluded that the remnants after the thermal test were carbon fibers. However, a lower value for recycled fibers (PLA/SCF_R) may result from a lower real weight concentration of the modifier in the polymer. During the filament manufacturing, some of the fibers could have been deposited in the extruder chamber, thereby not mixing with the polymer.

Photographs of printed dogbone shape samples are presented in FIG. 12. The quality of the printed samples shows that the obtained filaments can be used in a 3D printer. The sample with the best quality is PLA/SCF_R (FIG. 12C) - it can be seen that it does not significantly differ from the commercial sample (FIG. 12B). 3D printing of this material was carried out without major complications (FIG. 13).

The results of the tensile test of the dogbone shape samples are shown in TABLE 9. The highest tensile strength was observed for PLA/CNT. Relative strain and destructive work are also the highest in this case. Slightly worse of these parameters, although the higher Young's modulus was observed for PLA/SCF_R sample. For the nanocomposite PLA/GO, relatively low mechanical parameters were noted, which was also found in the study of PLA/GO filament. This is another confirmation of the lack of sufficient homogenization of the GO in polymers matrix. High relative strain value indicates that tensile stresses were mainly transmitted through the polymer matrix.

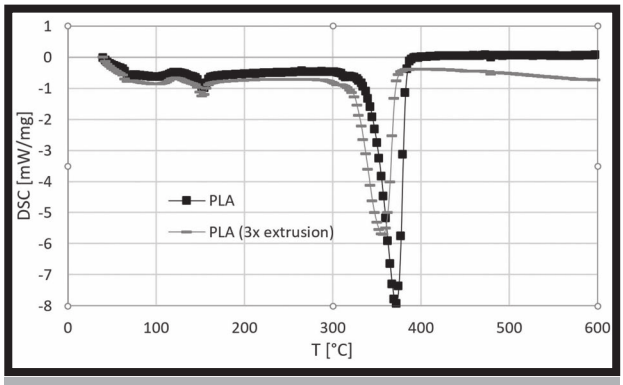

FIG. 9. DSC curve for PLA and PLA after triple extrusion.

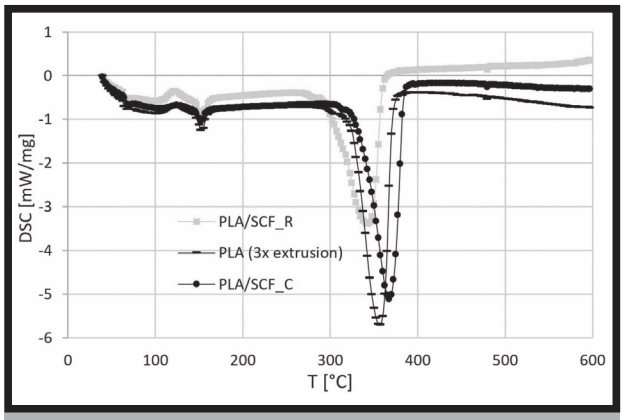

FIG. 10. DSC curves for PLA after triple extrusion and for composite filaments: PLA/SCF_R, PLA/SCF_C.

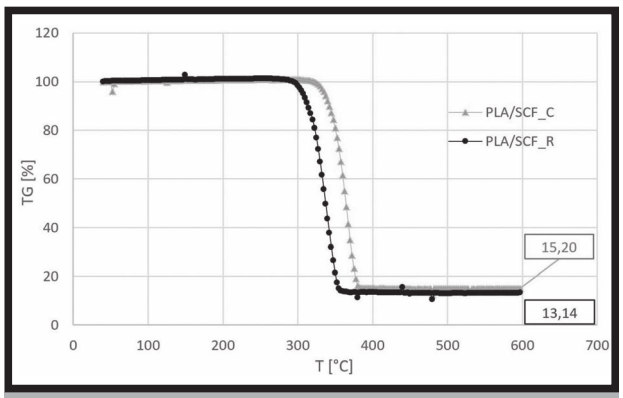

FIG. 11. TG curve for PLA/SCF_R, PLA/SCF_C samples.

FIG. 12. 3D printed dogbone shape samples: A) PLA, B) PLA/SCF_C, C) PLA/SCF_R, D) PLA/GO, E) PLA/CNT.

FIG. 13. Hexagonal infill (20%) of the PLA/SCF_R sample.

TABLE 9. Results of tensile test of the 3D printed samples.

	R_m ± SD [MPa]	Modulus ± SD [GPa]	Strain ε ± SD [%]	Rupture work ± SD [N·mm]
PLA	36.30 ± 3.63	1.23 ± 0.12	3.93 ± 0.39	698.94 ± 69.90
PLA/SCF_C	39.00 ± 0.57	2.10 ± 0.06	3.17 ± 0.15	648.61 ± 24.66
PLA/SCF_R	38.47 ± 6.21	2.02 ± 0.26	3.04 ± 0.21	633.75 ± 158.96
PLA/GO	31.68 ± 2.33	1.23 ± 0.07	3.62 ± 0.31	604.74 ± 101.19
PLA/CNT	38.98 ± 2.07	1.32 ± 0.08	4.07 ± 0.13	814.54 ± 80.01

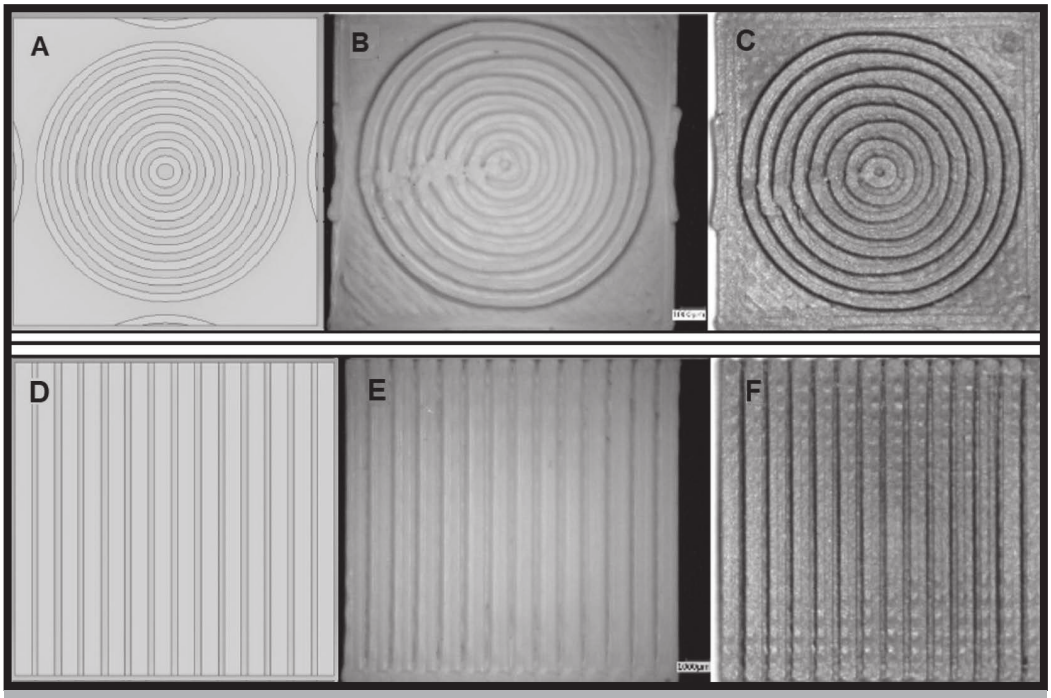

FIG. 14. Digital models and printed scaffolds: A) ring model, B) PLA ring scaffold, C) PLA/SCF_R ring scaffold, D) linear model, E) PLA linear scaffold, F) PLA/SCF_R linear scaffold.

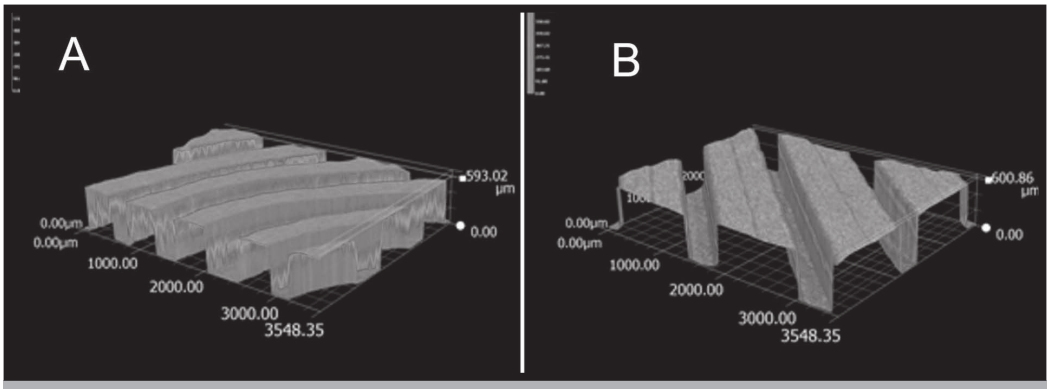

FIG. 15. 3D images of microstructure of printed scaffolds: A) ring, B) linear.

3D printing of scaffolds

After optimizing the printing process, 3D prints of the pure PLA scaffolds and composites scaffolds obtained from PLA/SCF_R filament were made. The choice of this composite material for printing of the scaffolds resulted from the analysis of results for all filaments and dogbone shape samples. Filament PLA/SCF_R was characterized by the highest quality as well as optimal mechanical parameters. Also, the PLA/SCF_R dogbone shape samples showed the most favorable properties. FIG. 14 presents photographs of 3D scaffolds printed from PLA and PLA/SCF_R filaments with images of digital models of individual designs. The obtained scaffolds retain their designed shape, however, greater dimensional stability is shown by the linear structure than the ring structure. The dimensional analysis made on digital microscope allowed to obtain 3D images of printed scaffolds (FIG. 15). The calculations based on digital visualization show that the real height of the PLA/SCF_R ring and linear structures is smaller than the assumed by 30% and 17%, respectively (FIG. 16). The lower value of the height of the printed paths in scaffolds results most probably from the spreading of the melted polymer bundle of due to the action of gravity. This effect should be taken into account when designing further scaffolds.

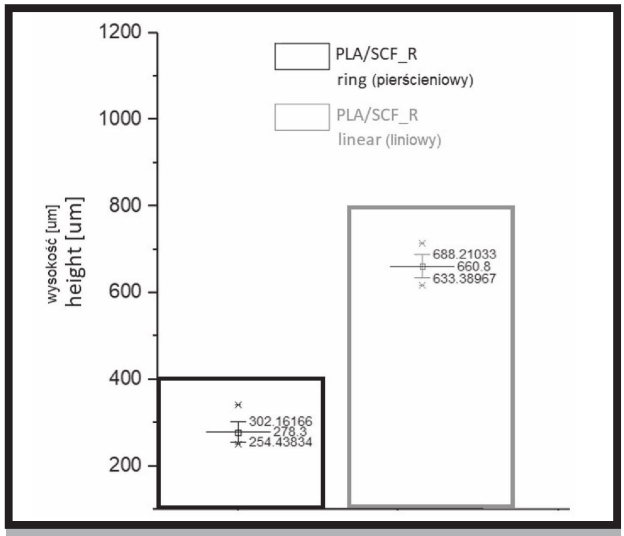

FIG. 16. Results of the analysis of topography changes in PLA/SCF_R scaffolds - average values, standard deviations and outliers; bar charts show the expected values in accordance with the project.

Conclusions

This paper presents the 3D printing process using the FDM method, starting from the selection of materials, through the complicated filament production procedure, to its use in a 3D printer, as well as optimizing the printing process and obtaining the desired objects. Based on the conducted experiments, it can be concluded that the whole process is quite complex, requires knowledge and experience demanding experience without which it is practically impossible to obtain high-quality materials. Despite numerous difficulties during filament production and 3D printing, composite printing is possible, and if the filament formation process will be optimized and the materials will be properly homogenized, the entire technology of self-generation of composite and nanocomposite objects with a polymer matrix using the 3D printing method can be fast and very effective. In addition, it is highly desirable to use recycled materials, so the method has both economic and ecological benefits. Moreover, the possibility of using biodegradable and biocompatible with the human body materials makes this technology has potential and can be an alternative in producing prototypes and forming scaffolds for tissue engineering.

Acknowledgments

The study was financed from the statute funds of AGH-UST, Faculty of Materials Science and Ceramics, Project no. 11.11.160.182.

References

[1] E. Bayraktar: Reference Module in Materials Science and Materials Engineering. Composites Materials, Elsevier (2017)
[2] M. Ramalingam, S. Ramakrishna: Nanofiber Composites for Biomedical Applications. Elsevier (2017)
[3] G. Turnbull et al.: 3D bioactive composite scaffolds for bone tissue engineering. Bioactive Materials 3(3) (2018) 278-314.
[4] M.S. Scholz et al.: The use of composite materials in modern orthopaedic medicine and prosthetic devices: A review. Composite Science and Technology 71(16) (2011) 1791-1803.
[5] I. Armentano et al.: Multifunctional nanostructured PLA materials for packaging and tissue engineering. Progress in Polymer Science 38, (10-11) (2013) 1720-1747.
[6] I.J. Macha et al.: In vitro study and characterization of cotton fabric PLA composite as a slow antibiotic delivery device for biomedical applications. Journal of Drug Delivery Science and Technology 43 (2018) 172-177.
[7] Y. Liu et al.: Composite poly(lactic acid)/chitosan nanofibrous scaffolds for cardiac tissue engineering. International Journal of Biological Macromolecules 103 (2017) 1130-1137.
[8] C. Zhao et al.: Development of PLA/Mg composite for orthopedic implant: Tunable degradation and enhanced mineralization. Composites Science and Technology 147 (2017) 8-15.
[9] S. Tajbakhsh, F. Hajiali: A comprehensive study on the fabrication and properties of biocomposites of poly(lactic acid)/ceramics for bone tissue engineering. Materials Science and Engineering: C 70, Part 1, (2017) 897-912.
[10] C. Yang et al.: A facile electrospinning method to fabricate polylactide/graphene/MWCNTs nanofiber membrane for tissues scaffold. Applied Surface Science 362 (2016) 163-168.
[11] S. Jatteau et al.: A tubular polycaprolactone/hyaluronic acid scaffolds for nasal cartilage tissue engineering. Engineering of Biomaterials 141 (2017) 8-12.
[12] S. Yildirim et al.: Preparation of polycaprolactone/graphene oxide scaffolds: A green route combining supercritical CO_2 technology and porogen leaching. The Journal of Supercritical Fluids 133, Part 1 (2018) 156-162.
[13] E. Murray et al.: Enzymatic degradation of graphene/polycaprolactone materials for tissue engineering. Polymer Degradation and Stability 111 (2015) 71-77.
[14] E. Torres et al.: Improvement of mechanical and biological properties of Polycaprolactone loaded with Hydroxyapatite and Halloysite nanotubes. Materials Science and Engineering: C 75 (2017) 418-424.
[15] S. Mallakpour, N. Nouruzi: Polycaprolactone/metal oxide nanocomposites: An overview of recent progress and applications, Biodegradable and Biocompatible Polymer Composites (2018) 223-263.
[16] J.R. Dorgan et al.: Polylactides: properties and prospects of an environmentally benign plastic from renewable resources. Macromolecular Symposia 175(1) (2001) 55-66.
[17] E. Castro-Aguirre et al.: Poly(lactic acid)-Mass production, processing, industrial applications, and end of life. Advanced Drug Delivery Reviews 107 (2016) 333-366.
[18] D. da Silva et al.: Biocompatibility, biodegradation and excretion of polylactic acid (PLA) in medical implants and theranostic systems. Chemical Engineering Journal 340 (2018) 9-14.
[19] F.P. La Mantia et al.: Degradation of polymer blends: A brief review, Polymer Degradation and Stability 145 (2017) 79-92.
[20] N.S. Yatigala et al.: Compatibilization improves physico--mechanical properties of biodegradable biobased polymer composites. Composites Part A: Applied Science and Manufacturing 107 (2018) 315-325.
[21] P. Huang et al.: 3D printing of carbon fiber-filled conductive silicon rubber. Materials & Design 142 (2018) 11-21.
[22] R.T.L. Ferreira et al.: Experimental characterization and micrography of 3D printed PLA and PLA reinforced with short carbon fibers. Composites Part B: Engineering 124 (2017) 88-100.
[23] E. Murray et al.; Enzymatic degradation of graphene/polycaprolactone materials for tissue engineering. Polymer Degradation and Stability 111 (2015) 71-77.
[24] A. Pantano: Mechanical Properties of CNT/Polymer, Carbon Nanotube-Reinforced Polymers, From Nanoscale to Macroscale, Micro and Nano Technologies (2018) 201-232.
[25] K. Kim et al.: 3D printing of multiaxial force sensors using carbon nanotube (CNT)/thermoplastic polyurethane (TPU) filaments. Sensors and Actuators A: Physical 263 (2017) 493-500.
[26] K. Mitura, P.K. Zarzycki: Biocompatibility and Toxicity of Allotropic Forms of Carbon in Food Packaging, Role of Materials Science in Food Bioengineering. Handbook of Food Bioengineering (2018) 73-107.
[27] N.G. Shimpi: Biodegradable and Biocompatible Polymer Composites - Processing, Properties and Applications. Composite Science and Engineering (2017)
[28] N. Aliheidari et al.: Fracture resistance measurement of fused deposition modeling 3D printed polymers. Polymer Testing 60 (2017) 94-101.
[29] Y. Deng, J. Kuiper: Extrusion-based 3D printing technologies for 3D scaffold engineering, Functional 3D Tissue Engineering Scaffolds - Materials, Technologies and Applications (2017)
[30] M. Guvendiren et al.: Designing Biomaterials for 3D Printing, ACS Biomaterials Science & Engineering 2(10) (2016) 1679-1693.
[31] www.barrus.pl (10.02.2018)
[32] www.nanoamor.com (28.08.2018)